Journal of Materials Chemistry A

PAPER

Check for updates

Cite this: J. Mater. Chem. A, 2019, 7, 11934

Rhodium nanoparticles supported on covalent triazine-based frameworks as re-usable catalyst for benzene hydrogenation and hydrogen evolution reaction†

Marvin Siebels,[a] Carsten Schlüsener,[a] Jörg Thomas,[b] Yu-Xuan Xiao,[c] Xiao-Yu Yang[c] and Christoph Janiak[*ad]

Received 22nd December 2018
Accepted 14th April 2019

DOI: 10.1039/c8ta12353e

rsc.li/materials-a

Metal nanoparticles (M-NPs) of ruthenium, rhodium, iridium and platinum were synthesized and supported on covalent triazine-based framework from 1,4-dicyanobenzene (CTF-1) by rapid microwave induced decomposition of their binary metal(0) carbonyls for Ru, Rh and Ir or $Pt(acac)_2$ in the presence of CTF-1 in the ionic liquid (IL) 1-butyl-3-methylimidazolium bis(trifluoromethylsulfonyl)imide ([BMIm][NTf_2]) or in propylene carbonate (PC). (High-resolution) transmission electron microscopy, (HR-)TEM showed the formation of M-NPs on CTF-1 with, *e.g.*, size distributions of 3.0 (±0.5) nm for Ru@CTF-1 synthesized in [BMIm][NTf_2] and 2 (±1) nm for Rh@CTF-1 synthesized in PC. The crystalline phases of the M-NPs and the absence of significant impurities were verified by powder X-ray diffraction (PXRD) and selected area electron diffraction (SAED). The metal content of the M@CTF-1 composites was determined by flame atomic absorption spectroscopy (AAS) to be between 3 and 12 wt%. The Rh@CTF-1 composite nanomaterial proved to be a highly active (~31 000 mol cyclohexane per (mol Rh) per h) heterogeneous catalyst for the hydrogenation of benzene to cyclohexane under mild (10 bar H_2, 70 °C) and solvent-free conditions with over 99% conversion. The catalyst could be re-used for at least ten consecutive hydrogenation reactions. Additionally, Rh@CTF-1 is an active electrocatalyst for the hydrogen evolution reaction (HER) with an operating potential of −58 mV, while Pt@CTF-1 and commercial Pt/C shows a more negative operating potential of −111 and −77 mV. Also the onset potential of −31 mV for Rh@CTF-1 is much more positive than that of Pt@CTF-1 (−44 mV) and commercial Pt/C (−38 mV).

Introduction

The hydrogenation of benzene to cyclohexane has been studied extensively and is of great interest in the petroleum industry and for the industrial production of cyclohexane.[1–4] In diesel fuel the aromatic content needs to be removed by hydrogenation to fulfil environmental regulations.[5] Cyclohexane is important for the synthesis of fine chemicals[6] and is used, for example, as a precursor for the production of nylon-6 and nylon-66.[7] In addition, cyclohexane is a very good solvent, with a lower toxicity than benzene.[8]

Ruthenium,[9,10] rhodium[10–12] and palladium[13,14] are often used in catalytic reactions in nanoparticle form in order to enhance the metal-based catalytic activity by the exposed high surface area of the small particles.[15–18] The abovementioned metals often show high catalytic activity under mild reaction conditions and are frequently recyclable.[19–21] Especially, Rh-NPs are known for their very high catalytic activity in the hydrogenation of unsaturated compounds, in Fischer–Tropsch synthesis and for steam reforming processes in hydrocarbons.[22–25]

Covalent triazine-based frameworks (CTFs) represent a class of highly stable microporous polymers first described in 2008 by Kuhn *et al.* (Scheme 1).[26,27] In particular, CTFs feature a high specific surface area, high porosity, high degree of graphitization and are chemically and thermally stable.[28,29] According to their physiochemical properties, easy access[30,31] and chemical variability[32] there is an increasing interest of CTFs in catalysis,[33,34] gas storage/separation and extraction,[30,35] as well as in energy storage.[36,37]

[a]Institut für Anorganische Chemie und Strukturchemie, Heinrich-Heine-Universität Düsseldorf, 40204 Düsseldorf, Germany. E-mail: janiak@uni-duesseldorf.de; Fax: +49-211-81-12287; Tel: +49-211-81-12286

[b]Department Structure and Nano-/Micromechanics of Materials, Max-Planck-Institut für Eisenforschung GmbH, 40237 Düsseldorf, Germany

[c]State Key Laboratory of Advanced Technology for Materials Synthesis and Processing, Wuhan University of Technology, 430070 Wuhan, China

[d]Hoffmann Institute of Advanced Materials, Shenzhen Polytechnic, 7098 Liuxian Blvd, Nanshan District, Shenzhen, China

† Electronic supplementary information (ESI) available: Synthesis and characterization of CTF-1, structural formula of the ionic liquid (IL) and propylene carbonate (PC), synthesis and characterization of the CTF-1-supported NPs, and hydrogenation of benzene and cyclohexene. See DOI: 10.1039/c8ta12353e

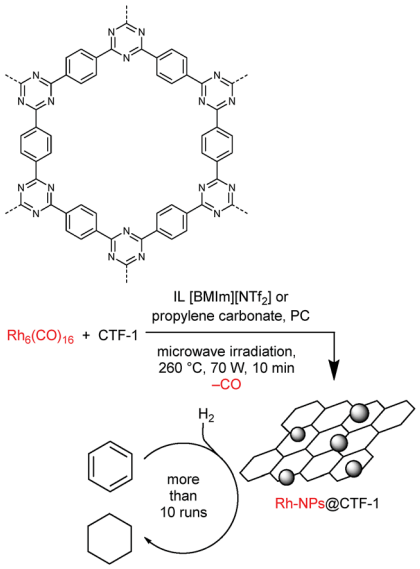

Scheme 1 Idealized structure of CTF-1 with triazine-rings and hexagonal openings in 2D network (top) and the synthesis of Rh@CTF-1 composite nanomaterial from $Rh_6(CO)_{16}$ by microwave-assisted thermal decomposition in the presence of CTF-1 and catalytic hydrogenation reaction of benzene to cyclohexane (bottom).

The triazine rings, residual nitrile groups and other nitrogen groups formed during the reaction can function as anchor groups to support or coordinate catalytically active metal species.[38,39] Schüth *et al.* synthesized a platinum-modified CTF (CTF-Pt) by subsequent platinum coordination.[40] The material was used for the catalytic methane oxidation to methanol and yield high catalytic activity.[40] Chen *et al.* used CTF-1 from 1,4-dicyanobenzene for the immobilization of Pd-NPs.[41] In comparison to conventional catalysts, the resulting composite nanomaterial Pd/CTF proved to be very active for the hydrogenation of *N*-heterocycles.[41] Palkovits *et al.* coordinated molecular rhodium complexes within different CTFs (Rh@CTF) and used the material for the solvent-free hydroformylation of 1-octene.[42] The rhodium-CTF coordinated catalysts were not as active as conventional catalysts, however, their activity clearly exceeded comparable rhodium-on-carbon catalysts.[42] To the best of our knowledge, there is no report of rhodium nanoparticles supported on CTF, moreover, there are only two reports of CTF-supported metal nanoparticles[41,43] compared to coordinated metal complexes[44–46] and metal oxide nanoparticles.[47,48] Herein, we present a new and highly active Rh nanoparticle catalyst supported and stabilized on CTF-1 (Rh@CTF-1) for the hydrogenation of benzene to cyclohexane (Scheme 1) and for the hydrogen evolution reaction (HER).

Experimental section

Materials and methods

Hexarhodium(0) hexadecacarbonyl, $Rh_6(CO)_{16}$ (98%) was obtained from ABCR, triruthenium dodecacarbonyl, $Ru_3(CO)_{12}$ (99%) from Acros Organics, tetrairidium dodecacarbonyl, $Ir_4(CO)_{12}$ (98%) and zinc chloride, $ZnCl_2$ (>98%) from Alfa Aesar, platinum(II) acetylacetonate, $Pt(acac)_2$ (97%) from Sigma Aldrich, benzene (p.A.) from Merck and bis(trifluoromethane)-sulfonimide lithium salt (99%) from ABCR and used without further purification. 1,4-Dicyanobenzene (98%) was purchased from Sigma Aldrich, purified by recrystallization in ethanol and then dried under high vacuum (10^{-3} mbar). Propylene carbonate (PC) was obtained from Sigma Aldrich (99.7%) and was dried under high vacuum for a few days. 1-Chlorobutane (>99%) and 1-methylimidazole (>99%) were obtained from Sigma Aldrich and purified by fractional distillation, then dried over 4 Å molecular sieves for several days.

Elemental (CNH) analyses were carried out with a Perkin-Elmer 2400 series 8 elemental analyser.

Flame atomic absorption spectroscopy (AAS) for metal analyses were performed on a Vario 6 from Analytik Jena.

Conversion of benzene to cyclohexane was determined by headspace gas chromatography (GC) (Perkin-Elmer 8500 HSB 6, equipped with a DB-5 film capillary column, 60 m × 0.32 mm, film thickness 25 μm, oven temperature 33 °C, N_2 carrier flow 105 L min^{-1}, 180 °C injection temperature, 75 °C auxiliary gas temperature and a flame ionization detector (FID), 250 °C detector temperature).

Powder X-ray diffraction, PXRD data were measured at ambient temperature on a Bruker D2-Phaser using a flat sample holder and Cu-Kα radiation ($\lambda = 1.54182$ Å, 35 kV). Samples had been precipitated with acetonitrile from the NP/IL dispersion and washed several times with acetonitrile. PXRDs were measured for 1 h. Small shifts in PXRD patterns are not uncommon for nanoparticles. A number of effects can be considered for such shifts including range of stoichiometric composition, partly inhomogeneous element distribution, defects such as stacking and twin faults and nanosized crystalline domains being much smaller than the bulk reference material causing lattice contraction or expansion and strain.[49–53]

Scanning electron microscopy (SEM) images were acquired on a JEOL JSM-6510 Advanced electron microscope (Jeol, Akishima, Japan) with a LaB_6 cathode at 5–20 keV. The microscope was equipped with a XFlash 410 (Bruker, Billerica, US) silicon drift detector.

Selected area electron diffraction (SAED) patterns have been recorded with an FEI Tecnai G2 F20 TEM,[54] operated at 200 kV accelerating voltage. The area selection was achieved with a round aperture placed in the first intermediate image plane with a corresponding diameter of 0.64 μm in the object plane. For each acquisition, a sample region with a significant amount of material was placed inside the aperture. The objected was illuminated with wide-spread parallel beam obtaining focused diffraction patterns. The diffraction images were calibrated with Debye–Scherrer patterns recorded from a gold reference sample (S106, Plano GmbH, Wetzlar, Germany).

Surface areas (BET) were determined by nitrogen (purity 99.999%, 5.0) sorption experiments at 77 K using liquid nitrogen and approx. 20–50 mg of the sample, performed on a Quantachrome NOVA-4000e (Quantachrome, Odelzhausen, Germany) instrument within a partial pressure range of $P/P_0 = 10^{-3}$ – 1 bar. Each sample was degassed under vacuum (<10^{-2} mbar) at 120 °C for approx. 3 h prior to measurement. All the

surface areas (BET) were calculated from five adsorption points applying Roquerol plots ($r > 0.998$).

Thermogravimetric analysis (TGA) was carried out on a Netzsch TG209 F3 Tarsus (Netzsch, Selb, Germany) device under a nitrogen atmosphere, ramping at 5 K min^{-1} to 1000 °C.

Transmission electron microscopy, TEM was performed with a FEI Tecnai G2 F20 electron microscope operated at 200 kV accelerating voltage.[54] Conventional TEM images were recorded with a Gatan UltraScan 1000P detector. TEM samples were prepared by drop-casting the diluted material on 200 μm carbon-coated copper grids or gold grids. The size distribution was determined manually or with the aid of the Gatan Digital Micrograph software from at least 50 individual particles. EDX spectra for composition analysis were recorded with the same instrument using an exposure time of 3 min.

High-resolution micrographs were recorded with an FEI Titan 80-300 transmission electron microscope[55] operated at 300 kV accelerating voltage. The instrument is equipped with a field emission gun and a corrector for the spherical aberration (CS) of the imaging lens system providing a spatial resolution of better than 0.1 nm, limited by chromatic aberration.[56] The images were acquired with a 2 k × 2 k GATAN UltraScan 1000 CCD. By applying the NCSI technique with a small negative CS of 14 μm and a few nanometers overfocus a strong image contrast is obtained that is localized as much as possible at the atomic columns.[57] The residual lens aberrations of the microscope were measured by the Zemlin tableau method and minimized shortly before the image acquisition.[58] High-resolution (HR-) images of Rh-NPs could be obtained at the edge of the CTF-1 flakes. Only in this region the contrast allowed to obtain such HR-TEM images.

Synthesis of CTF-1

Covalent triazine-based framework from 1,4-dicyanobenzene (CTF-1) was synthesized according to the literature procedure.[59] Anhydrous zinc chloride (1.63 g, 0.012 mol, 5 eq.) and 1,4-dicyanobenzene (0.308 g, 2.4×10^{-4} mol, 1 eq.) were mixed under inert conditions in a glass ampoule. The ampoule was evacuated, sealed and heated at 400 °C for 48 h. The black product was removed from the vial, mortared and stirred with 250 mL ultrapure water for 96 h. The product was isolated by filtration and stirred with 200 mL of dilute hydrochloric acid (2 mol L^{-1}) for 24 h. The resulting black powder was further washed with de-ionized water (3 × 75 mL), THF (3 × 75 mL), acetone (3 × 75 mL) and dried under ultra-high vacuum (10^{-7} mbar) at 70 °C for 72 h.

Synthesis of [BMIm][NTf_2]

The ionic liquid (IL), 1-butyl-3-methylimidazolium bis(trifluoromethylsulfonyl)imide ([BMIm][NTf_2]) were synthesized by reacting 1-methylimidazole with 1-chlorobutane to yield [BMIm][Cl]. The [BMIm][Cl] reacted with $LiNTf_2$ to give [BMIm][NTf_2].[60] The IL was dried under ultra-high vacuum (10^{-7} mbar) at 70 °C for several days. The characterization was carried out by ^{1}H- and ^{13}C-NMR. Quantitative anion exchange and, thus, IL purity was assessed by ion chromatography (Dionex ICS-1100, with IonPac® AS22, 4 × 250 mm column) to be >99% for the IL. The water content by coulometric Karl Fischer titration was less than 10 ppm.

Synthesis of Rh@CTF-1 nanoparticles in [BMIm][NTf_2] or PC

$Rh_6(CO)_{16}$ (8.6 mg, 8.1×10^{-3} mmol) together with 10 mg of CTF-1 (1 wt% related to 1 g of IL or PC) were dispersed in the dried IL or in PC at room temperature with magnetic stirring for 24 h in a microwave reaction vial under argon atmosphere. Mass of the metal was set for a 0.5 wt% Rh-NP in IL or PC dispersion. The mixture was placed in a microwave (CEM, Discover) and irradiated for 10 min at a power of 70 W to a temperature of 260 °C. The volatiles (CO) were removed under vacuum and the black dispersion washed with acetonitrile (4 × 5 mL) and centrifuged. Finally, the Rh@CTF-1 nanomaterials were dried under vacuum for several hours (yield 13.1 mg, 87.5% for Rh@CTF-1/IL and 12.6 mg, 84% for Rh@CTF-1/PC). From a mass balance of the used starting materials (8.6 mg of the Rh-carbonyl compound and 10 mg CTF) in combination with the AAS determination of the Rh content in Rh@CTF-1 it is evident that only a small part of the available Rh metal is deposited on CTF-1. Further, the yield of the Rh@CTF-1 products (13.1 mg in IL and 12.6 mg in PC) is higher than expected from the 10 mg CTF-1 amount of the starting material with only ~5 wt% Rh. The excess weight can be assigned to IL or PC within the Rh@CTF-1 material. We know from TEM investigations that even after the extensive washing process of the Rh@CTF-1 material, a small amount or residual IL/PC layer adheres to the NPs and inside the remaining pores of CTF-1.

Hydrogenation reactions

All catalytic processes were done using stainless-steel autoclaves under inert atmosphere. Each autoclave was equipped with a glass inlay to avoid any effect of the steel in the reaction. The desired amount of catalyst (Rh@CTF-1 from [BMIm][NTf_2], 4 mg containing 4.4 wt% Rh, 1.73×10^{-3} mmol Rh; Rh@CTF-1 from PC, 3 mg containing 6.1 wt% Rh, 1.73×10^{-3} mmol Rh) together with the substrate (benzene, 1 mL, 0.87 g, 11.14 mmol) were loaded in the autoclave. The autoclave was purged three times with H_2 and heated to 70 °C. Once the set temperature was achieved, the autoclave was charged with 10 bars of H_2 and the mixture was stirred (800 rpm). H_2-uptake measurements were followed with a Büchi bpc pressflow controller. After catalytic reactions the autoclave was cooled down and depressurized. The volatile organic content was isolated by evaporation and condensation under vacuum in a cold trap. Conversion of benzene to cyclohexane was determined by GC. The catalyst could be recovered and re-used for at least 10 times. All procedures were repeated at least twice to evaluate the reproducibility of the process.

Hydrogen evolution reaction

The electrochemical measurement was tested on an Autolab working station from Metrohm, Switzerland. A three-electrode cell was used to conduct the electrochemical measurements. A platinum mesh was used as a counter electrode and a Ag/AgCl

electrode was used as a reference electrode. The working electrode was a glassy-carbon Rotating Disk Electrode (RDE, diameter: 5 mm, area: 0.196 cm^2). The Pt loading in the commercial Pt/C material is 20%. Both mass loading of Rh and Pt for Rh@CTF-1, Pt@CTF-1 and Pt/C on glassy-carbon were 3.0 μg. Polarization curves were collected in 0.5 M H_2SO_4 solutions at a rotation rate of 1600 rpm with a sweep rate of 20 mV s^{-1}.

Results and discussion

Synthesis and characterization of Rh@CTF-1

The synthesis and characterization of the covalent triazine-based framework CTF-1 from 1,4-dicyanobenzene was carried out according to ionothermal literature procedures (400 °C in $ZnCl_2$; see Scheme S1, Fig. S2, Table S3, Fig. S4 and S5 in ESI† for details).[59]

Rhodium nanoparticles (Rh-NPs) were synthesized and supported simultaneously on CTF-1 by microwave irradiation (260 °C, 70 W, 10 min) of hexarhodium(0) hexadecacarbonyl, $Rh_6(CO)_{16}$ in the presence of CTF-1 (Scheme 1). As reaction media we used the ionic liquid (IL) 1-butyl-3-methylimidazolium bis(trifluoromethylsulfonyl)imide ([BMIm][NTf_2]) or the organic solvent propylene carbonate (PC) (Fig. S7 in ESI†).

In the last decades, ILs are increasingly used in the synthetic of inorganic materials.[61,62] The liquids salts are used within M-NPs synthesis mostly as reaction media and stabilizing reagents,[63,64] seldom also as fluorine- or selenium-containing reactants for metal fluoride or metal selenide nanoparticle syntheses.[65,66] In contrast to coordinating stabilizers, such as capping ligands, surfactants or donor-atom containing polymers, ILs stabilize M-NPs through electrostatic and steric interactions. The weakly coordinating cations and anions of the IL should only little alter the surface properties of the particles.[67]

Propylene carbonate, PC is an aprotic and strongly dipolar solvent with low viscosity, low flammability and low toxicity.[68] PC is used, for example, as a solvent for lithium ion batteries, as a solubilizer and co-solvent in cosmetics and lacquer.[69] PC is also known as a solvent and stabilizing reagent for M-NPs synthesis.[70]

The size regimes of the achieved Rh-NPs were determined by (high-resolution) transmission electron microscopy, (HR-)TEM to values of 1–4 nm giving average diameters of 3 (±1) nm for Rh@CTF-1 synthesized in [BMIm][NTf_2] (Fig. 1) and 2 (±1) nm for Rh@CTF-1 synthesized in PC (Fig. S9 in ESI†). The TEM images also verify the successful and even deposition of the nanoparticles on CTF-1.

The even Rh-NP immobilization on CTF-1 is also shown through scanning electron microscopy (SEM) in combination with energy-dispersive X-ray spectroscopic (EDX) elemental mapping analysis (Fig. 2 and S11 in ESI†).

The Rh metal content of the Rh@CTF-1 composites material was determined by flame atomic absorption spectroscopy (AAS) to 4.4 wt% for Rh@CTF-1 synthesized in [BMIm][NTf_2] and to 6.1 wt% for Rh@CTF-1 synthesized in PC.

The crystallinity of the Rh-NPs was confirmed by powder X-ray diffraction (PXRD) and the crystal phase positively

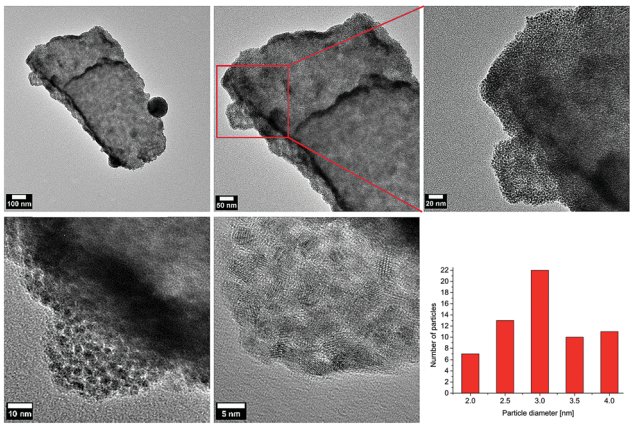

Fig. 1 TEM (upper row) and HR-TEM (lower row) images and particle size histogram from 53 particles of Rh@CTF-1 composite synthesized in [BMIm][NTf_2] using microwave irradiation. TEM and HR-TEM images were taken on different positions on the TEM grid of the same sample. For the EDX analysis in combination with TEM see Fig. S10 in ESI.†

matched to as cubic Rh metal (Fig. 3 and S12 in ESI†). The diameters of the Rh-NPs were also derived from evaluation of as many reflections as possible in the PXRD by using the Scherrer equation to values of 5–6 nm for Rh@CTF-1 synthesized in [BMIm][NTf_2] and 3–5 nm for Rh@CTF-1 synthesized in PC. Additionally, the crystalline phase of Rh metal was also verified by selected area electron diffraction (SAED) (Fig. 3 and S12 in ESI†). In addition, close-up HR-TEM images show interference patterns for Rh-NPs@CTF-1, which also indicate crystallinity of the samples (Fig. 1 and S9 in ESI†).

Similar experiments with triruthenium(0) dodecacarbonyl, $Ru_3(CO)_{12}$, tetrairidium(0) dodecacarbonyl, $Ir_4(CO)_{12}$ and platinum(II) acetylacetonate in the ILs 1-butyl-3-methylimidazolium tetrafluoroborate ([BMIm][BF_4]), [BMIm][NTf_2] or in PC gave Ru@CTF-1, Ir@CTF-1 and Pt@CTF-1, respectively (Scheme S8 in ESI†). TEM in combination with EDX analysis, SAED and PXRD measurements (see Fig. S13–S17 in ESI† for details) also yield small nanoparticles (<10 nm), which are supported on CTF-1. However, the catalytic hydrogenation of these supported Ru, Ir and Pt nanoparticles was not as active and reproducible as with Rh@CTF-1 (see below).

Hydrogenation of benzene

All M@CTF-1 probes were tested as catalysts in the hydrogenation of benzene (Tables 1 and S19 in ESI†) as well as

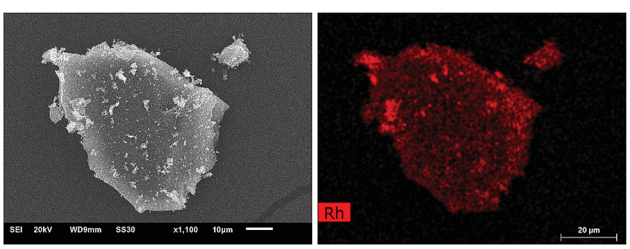

Fig. 2 SEM image (left) and Rh EDX mapping analysis (right) of Rh@CTF-1 composite nanomaterials synthesized in [BMIm][NTf_2].

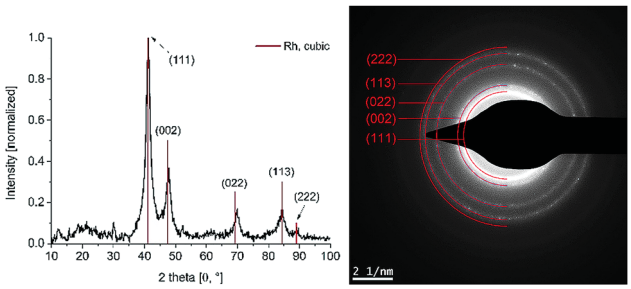

Fig. 3 PXRD and SAED (Rh reference peaks in red from COD 9008482, cubic structure) of Rh@CTF-1 synthesized in [BMIm][NTf_2]. From the PXRD the Rh-NP diameter was calculated with the Scherrer equation to 5–6 nm (Scherrer factor = 0.9; anisotropic defects were not considered; a range is given for diameter values derived from different reflections).

cyclohexene (Table S20 in ESI†). Ru@CTF-1 gave near quantitative conversion in at least 127 min and yielded TOF values up to ~3000 h^{-1} (Table S19 in ESI†) whereas Rh@CTF-1 even reached near quantitative conversion in about 13 min with TOF values up to ~31 000 h^{-1} (Table 1) for the hydrogenation of benzene to cyclohexane. After at least 3 hours, no hydrogen uptake was detected for the hydrogenation of benzene with Ir@CTF-1 and Pt@CTF-1 (Table S19 in ESI†). However, Ru@CTF-1, Ir@CTF-1 and Pt@CTF-1 showed high catalytic activity for the hydrogenation of cyclohexene to cyclohexane (Table S20 in ESI†).

Table 1 Catalytic hydrogenation of benzene to cyclohexane with Rh@CTF-1 composite nanomaterials[a]

Catalyst[b]	Run[a]	Conversion [%][c]	Time [min][d]	TOF [h^{-1}][e]
Rh@CTF-1/IL[f]	1	>99	27	14 489
	2	>99	31	12 636
	3	>99	33	11 855
	4	>99	34	11 643
	5	>99	37	10 585
	6	>99	36	10 867
	7	>99	43	9106
	8	>99	41	9546
	9	>99	44	8931
	10	>99	45	8964
Rh@CTF-1/PC[g]	1	>99	13	31 049
	2	>99	15	26 081
	3	>99	16	25 078
	4	>99	14	28 349
	5	>99	15	26 081
	6	>99	16	25 078
	7	>99	19	21 033
	8	>99	22	18 112
	9	>99	23	17 159
	10	96	23	16 472

[a] Each catalyst re-use sequence with 10 runs was repeated at least twice to ensure the reproducibility of the recycling process. The other run sequence deviated less than 10 min in IL and less than 2 min in PC for the time needed to achieve >99% conversion. This led to TOF values within 22% to each other. [b] Hydrogenation with Rh@CTF-1, (containing 1.73×10^{-3} mmol Rh) at a benzene/rhodium ratio of 6436, 70 °C, 10 bars H_2. [c] Calculation based on cyclohexane yield determined by headspace GC together with an H_2-uptake of 757 mL (33.4 mmol) corresponding to quantitative conversion of benzene (1.0 mL, 0.87 g, 11.14 mmol). [d] Time needed for the given conversion. [e] Turnover frequency (TOF) = activity as (mol cyclohexane) per (mol Rh) per h; with total quantity of Rh metal present in the nanomaterial. The turnover number (TON) = activity as (mol cyclohexane) per (mol Rh); with total quantity of Rh metal present in the nanomaterial was 6520 for each run. [f] Rh@CTF-1 catalyst synthesized in [BMIm][NTf_2], 4 mg containing 4.4 wt% Rh, 1.73×10^{-3} mmol Rh. [g] Rh@CTF-1 catalyst synthesized in PC, 3 mg containing 6.1 wt% Rh, 1.73×10^{-3} mmol Rh.

Subsequently, the most active Rh@CTF-1 composite nanomaterial was tested in more detail as a recyclable heterogeneous catalyst for the industrially relevant hydrogenation reaction of benzene to cyclohexane under mild and solvent-free conditions (Scheme 2).

Before catalytic reactions of benzene with Rh@CTF-1 as heterogeneous catalyst (Scheme 2), control experiments were performed under same conditions with the precursor $Rh_6(CO)_{16}$, CTF-1, [BMIm][NTf_2] and PC, albeit without giving any activity.

In a typical hydrogenation reaction Rh@CTF-1 powder and the benzene substrate were loaded in an autoclave. Once the set temperature of 70 °C (oil bath temperature) was achieved, the autoclave was charged with 10 bars of H_2. The H_2-uptake was monitored over time by a Büchi bpc press-flow controller. Once the H_2-uptake over time reached a plateau, the catalytic reaction was stopped and the volatile organic content was removed from the solid catalyst under vacuum into a cold trap. The catalytic activity of Rh@CTF-1 in the conversion of benzene to cyclohexane was evaluated by H_2-uptake over time (Table 1, Fig. 4 and S21 in ESI†) and by the calculated turnover frequency (TOF) (Table 1) and turnover number (TON). Quantitative conversion of benzene to cyclohexane and the absence of cyclohexene was verified by headspace gas chromatography (GC). Catalyst recycling was carried out by the above noted removal of the volatile organic content through the gas phase in vacuum and charging the autoclave with fresh benzene substrate under inert conditions. The catalyst Rh@CTF-1 can be recycled for at least ten times, with relatively little loss of activity (Table 1).

For the catalyst Rh@CTF-1 synthesized in [BMIm][NTf_2] (Rh@CTF-1/IL) or synthesized in PC (Rh@CTF-1/PC), it could be observed that the activity in the first runs are the highest with a more-or-less steady decrease generating a TOF maximum of ~31 000 h^{-1} near quantitative conversion in about 13 min for Rh@CTF-1/PC (Table 1, Fig. 4 and S21 in ESI†). However, the last runs of the catalytic hydrogenation still resulted to considerable TOF values up to ~9000 h^{-1} for Rh@CTF-1/IL and ~16 500 for Rh@CTF-1/PC.

For all the catalysis reactions, conversion rates above 99% were reached with TON of ~6500. For the evaluation of the catalytic activity as TOF and TON, the total quantity of rhodium

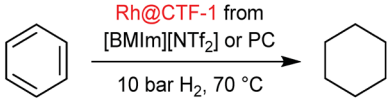

Scheme 2 Reaction scheme of the hydrogenation reaction of benzene to cyclohexane with Rh@CTF-1 as heterogeneous catalyst.

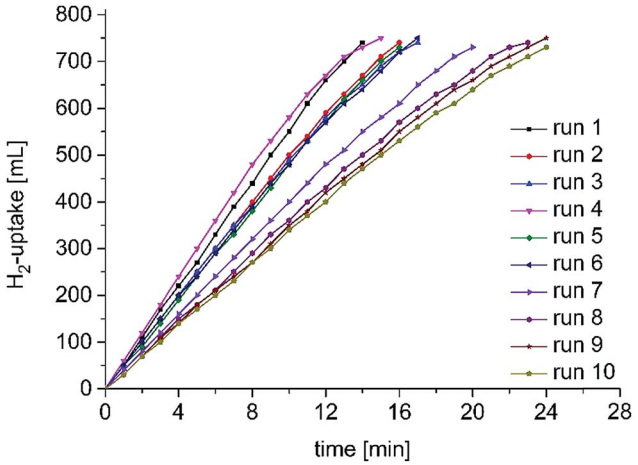

Fig. 4 H_2-uptake over time for the hydrogenation of benzene to cyclohexane with Rh@CTF-1 synthesized in PC.

atoms present in the composite nanomaterial was considered for calculation. We note that only surface atoms can be catalytically active with only a fraction of the surface atoms, such as corners or edges then being the active sites.[71]

For the hydrogenation of benzene to cyclohexane (Scheme 2), the catalyst Rh@CTF-1/IL reached a maximum conversion of >99% after 27 min, whereas the catalyst Rh@CTF-1/PC achieved a maximum conversion of >99% within 13 min (Table 1). The maximum TOF values for Rh@CTF-1/PC is 2.1-fold higher than the maximum TOF value for Rh@CTF-1/IL. This order of activity could be reproduced in two independent run sequences. We note that even after the washing process of the catalyst powder and IL, a small amount or residual IL layer remains around the nanoparticles. Brennecke *et al.* and Sahimi *et al.* investigated the solubility and diffusivity of H_2 in the ionic liquid 1-butyl-3-methylimidazolium hexafluorophosphate [BMIm][PF_6].[72,73] They found that hydrogen had very low solubilities and very low diffusivity in the IL.[72,73] We assume that the layer of [BMIm][NTf_2] around the nanoparticles in Rh@CTF-1/IL presents a diffusion barrier for the hydrogen substrate. This IL diffusion barrier slows down the catalytic reaction for Rh@CTF-1/IL when compared to Rh@CTF-1/PC.[9,10] The catalytic activity of nanomaterials depends, among other things, on their size and shape.[74,75] In comparison with Rh@CTF-1/IL, we obtained smaller Rh-NPs in the sample prepared in PC (3 ± 1 nm *vs.* 2.0 ± 0.5 nm). We note that the small particle size (more catalytic active surface atoms) of the Rh-NPs in Rh@CTF-1/PC leads to higher catalytic activity compared to Rh@CTF-1/IL (*cf.* Table 1).

The effect of the smaller particle size and, thus higher fraction of surface atoms was tried to take into account by estimating the number and fraction of surface atoms (see ESI†) and normalizing the TOF value to this fraction (TOF: fraction of surface atoms = TOF_{surf}). Taking the fraction of surface atoms into consideration yields TOF_{surf} values up to 34 498 h^{-1} for the IL and 58 583 h^{-1} for the PC material. Hence, the PC-derived material is still more active but on a relative scale it decreases to 1.7-fold (down from 2.1-fold when the total metal content was considered).

In addition, another two Rh@CTF-1 composite materials with higher amounts of Rh metal (8.6 wt% synthesized in [BMIm][NTf_2] (Fig. S22 in ESI†) and 15.9 wt% synthesized in PC (Fig. S23 in ESI†)) were prepared, characterized and tested for the hydrogenation of benzene to cyclohexane under same conditions (Table S24 and Fig. S25 in ESI†). The PXRD crystal phase was again positively matched to cubic Rh metal (Fig. S22 and S23, bottom right in ESI†). Particle size and dispersion was 3.0 ($\pm$0.5) nm in IL and 2.0 ($\pm$0.5) nm in PC. TEM images (Fig. S22 and S23, top in ESI†), for Rh@CTF-1/IL (8.6 wt%) and Rh@CTF-1/PC (15.9 wt%) showed densely loaded with Rh-NPs. It could be observed that the composite materials with about twice the metal content still proved to be highly active (TOF max. $\sim$ 11 000 h^{-1}) with quantitative conversion after 35 min but not as active as the Rh@CTF-1 composite (TOF max. $\sim$ 31 000 h^{-1}) with Rh metal loadings of 4.4 and 6.1 wt% (*cf.* Tables 1 and S24, ESI†). We rationalize the lower activity for the higher metal content by the dense loading which may restrict the access to the catalytic sites.

The hydrogenation of benzene to cyclohexane with nanoparticle catalysts has been extensively explored (Table S26 in ESI†). The focus is on the synthesis of nanoparticles supported on different materials such as silicon dioxide,[76] thermally reduced graphite oxide (TRGO),[10] metal–organic frameworks (MOFs),[77] polymers,[78] *etc.* Sánchez *et al.* reported the immobilization of Rh-NPs on magnesium oxide (Rh@MgO) applied for benzene hydrogenation, achieving a very high TOF of 81 000 h^{-1} under relatively mild conditions (100 °C, 10 bars H_2).[79] Bououdina *et al.* recently published a Rh nanoparticle catalyst deposited on iron oxide (Rh@Fe_3O_4) that show activities up to $\sim$300 h^{-1}.[80] Akbayrak recently published Rh-NPs supported on ceria (Rh@CeO_2) as a catalyst for benzene hydrogenation at room temperature.[81] Hydrogenation reactions with over 99% conversion were achieved under mild (3 bar H_2) and solvent-free conditions with TOF values up to 495 h^{-1}.[81] Trzeciak *et al.* prepared Rh-NPs stabilized by polyvinylpyrrolidone (PVP) (Rh/PVP-K30) that were catalytically active in hydrogenation of benzene in water under relatively mild conditions (80 °C, 20 bar H_2), yielding TOF values of 440 h^{-1}.[78] Xing *et al.* synthesized highly efficient Ru@SiO_2 nanocatalysts using a "porous" ionic liquid-water mixture.[76] The Ru@SiO_2 composite nanomaterial proved to be highly active (TOF 5000 h^{-1}) catalyst for benzene hydrogenation under relatively mild (100 °C, 20 bar H_2) and solvent-free conditions.[76] Furthermore, we investigated the catalytic activity of a commercial catalyst, where Rh was supported on activated charcoal (Rh@C), for benzene hydrogenation. Rh@C was a low active ($\sim$800 h^{-1}) catalyst for the hydrogenation of benzene compared to our Rh@CTF-1 composite nanomaterial (*cf.* Table S26 in ESI†). Of course, a true comparison of the catalysts is very difficult since the evaluation of the catalytic activity depends on many parameters (temperature, pressure, time, medium, *etc.*). TRGO supported metal nanoparticles were already investigated for the hydrogenation of benzene in our group for Ru,[9] Rh,[10] Ir,[15] and yield activities of 310 h^{-1} for Rh@TRGO, $\sim$10 000 h^{-1} for Ir@TRGO and $\sim$34 000 h^{-1} for Ru@TRGO (Table S26 in ESI†). In comparison with the literature, Rh@CTF-1

seems to be a very efficient and highly active catalyst with TOF values up to ~31 000 h^{-1} for the hydrogenation of benzene.

After ten consecutive hydrogenation runs, the catalyst Rh@CTF-1 was investigated by TEM (Fig. S27 in ESI† and Fig. 5), AAS measurements (Table 2), SEM-EDX elemental mapping analysis (Fig. S29 and S30 in ESI†), and SAED (Fig. S31 in ESI†). After the ten consecutive hydrogenation runs with Rh@CTF-1, there is a detectable aggregation or growth of the nanoparticles and a leaching effect which explains the reduction of the catalytic activity through the decrease of surface area and/or loss of metal (Table 1). The TEM images (Fig. S27 in ESI† and Fig. 5) show the enlargement of the Rh-NPs after catalysis from 3 (±1) to 6 (±3) nm for Rh@CTF-1/IL and 2 (±1) to 2.5 (±1) nm for Rh@CTF-1/PC (Table 2). The leaching was evident from AAS measurements. The metal content of rhodium in Rh@CTF-1 composite nanomaterial decreased from 4.4 to 3.5 wt% Rh for Rh@CTF-1/IL and from 6.1 to 4.9 wt% Rh for Rh@CTF-1/PC (Table 2). As any component removal is done through the gas phase and there are no liquid washing steps to the catalyst, we note that the decrease of the metal content from Rh@CTF-1 can also be caused by abrasion on the reactor walls or onto the stirring bar during catalysis.

From the SEM-EDX elemental mapping analysis of Rh@CTF-1 after catalysis the shard-like structure of the CTF-1 has remained unchanged and the rhodium metal is still rather evenly distributed on CTF-1 (Fig. S29 and S30 in ESI†).

According to SAED (Fig. S31 in ESI†), the crystalline phase of the Rh-NPs in Rh@CTF-1 after catalysis was again identified as cubic rhodium metal, albeit with significantly reduced crystallinity (*cf.* Fig. 3 and S12 in ESI†).

We assume that most of the immobilized Rh-NPs@CTF-1 with average diameters of 3 ± 1 nm for Rh@CTF-1/IL and 2.0 ± 0.5 nm for Rh@CTF-1/PC are adsorbed at the outer surface of the CTF flakes and not inside the porous network (pore diameter < 2 nm) of CTF-1. Evidence for this outer-surface adsorption was provided by (HR-)TEM images (Fig. 1 and S9, ESI†). Further, we reason the loss in catalytic activity by the particle aggregation and leaching because of this adsorption on the outer surface.

In order to prevent agglomeration- and leaching effects of Rh-NPs, it was further investigated whether the $Rh_6(CO)_{16}$ precursor could move into the pores of CTF-1 during an even longer dispersion time in IL/PC. The standard dispersion time before microwave-heating-induced precursor decomposition was 24 h. Therefore, we allowed the solid CTF-1 to interact with the $Rh_6(CO)_{16}$ precursor in IL or in PC for 7 days before microwave irradiation. The decomposition was carried out under the same conditions (260 °C, 70 W, 10 min). After the microwave decomposition, the nanoparticle size regimes of the achieved Rh-NPs were investigated by (HR-)TEM giving again average diameters of 3 ± 1 nm for Rh@CTF-1/IL (see Fig. S32 in ESI†) and 2.0 ± 0.5 nm Rh@CTF-1/PC (see Fig. S33 in ESI†). Even with a longer dispersion time of 7 days, the Rh-NPs@CTF-1 do not become smaller. Thus, most of the Rh-NPs are still adsorbed on the outer surface of the CTF-1 flakes. Thereby, we also note that ideally CTF-1 would have a 2D layer structure. During formation of the Rh-NPs by microwave heating the IL and PC do not only stabilize the NPs but can also exfoliate the CTF layers. The good contrast in the TEM images of the Rh@CTF-1 samples indicates that the CTF-1 flakes are around 10 nm (100 Å) thick. As a consequence of the exfoliation the BET porosity of bulk CTF-1 will no longer be available to the same extent and the outer surface area should increase strongly. Still, in comparison with the probe dispersed in IL for (only) 24 h, after the 7 days dispersion, the Rh-NPs of Rh@CTF-1/IL are more evenly distributed on the CTF-1 flakes as shown by TEM images (Fig. S32 in ESI†).

Table 2 Average diameter and Rh metal content of the Rh@CTF-1 composite nanomaterial before- and after ten consecutive runs in the hydrogenation of benzene to cyclohexane

	Before catalysis		After catalysis[a]	
Catalyst	Ø [nm][b]	Loading [wt%][c]	Ø [nm][b]	Loading [wt%][c]
Rh@CTF-1/IL[d]	3 (±1)	4.4	6 (±3)	3.5
Rh@CTF-1/PC[e]	2 (±1)	6.1	2.5 (±1)	4.9

[a] Measurements were taken after ten consecutive runs in the hydrogenation of benzene to cyclohexane with Rh@CTF-1 as heterogeneous catalyst. [b] Average diameter determined by using TEM images (Fig. S27 and S6 in ESI). [c] Rh metal content of the Rh@CTF-1 composite material determined with AAS measurements. [d] Rh@CTF-1 catalyst synthesized in [BMIm][NTf_2]. [e] Rh@CTF-1 catalyst synthesized in PC.

Often, NP suspensions are suspected to act as a reservoir for metal atoms/ions or molecular clusters that leach into solution where they can act as homogeneous catalysts.[82,83] To determine if the Rh@CTF-1 catalyst is indeed a heterogeneous system or if soluble, homogeneous Rh atoms/clusters which were set free from the Rh-NPs, were the active species, we added the rhodium catalyst poison CS_2 to the substrate according to a method described before.[84–86] As already mentioned, in a heterogeneous catalyst only the surface atoms and, thus, a small fraction of the metal content can be catalytically active (see ESI†).[71] Hence, for a heterogeneous catalyst it is possible to poison the catalyst completely with much less than 1 equiv. of CS_2.[84,87] For a homogeneous catalyst based on molecular species more than 1 equiv. of CS_2 should be needed to poison the catalyst. For Rh@CTF-1/IL or PC 0.42 or 0.53 equiv. CS_2 with respect to total Rh metal (corresponding to 1 equiv. CS_2 with respect to the surface atoms, see ESI† for the estimation of surface atoms) were added to the reaction mixture. Even after 3 hours no H_2-uptake was detected for the benzene hydrogenation.

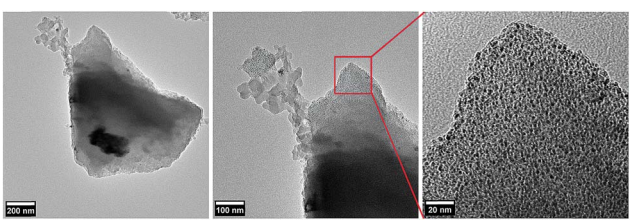

Fig. 5 TEM images of Rh@CTF-1 composite nanomaterials synthesized in PC after 10 hydrogenation runs. For additional TEM images after catalysis see Fig. S28 in ESI.†

To confirm additionally that Rh@CTF-1 catalyst is indeed a heterogeneous system and does not serve as a reservoir of a homogeneous catalyst based on molecular species, a filtration test was carried out with Rh@CTF-1/PC with 15.9 wt% Rh metal loading (Fig. S34 in ESI†). After stopping the catalysis at 14 min with 270 mL H_2-uptake (see Fig. S34, black line in ESI†), we separated the catalyst from the substrate by filtration (through a 0.2 μm syringe filter). Afterwards, we continued the hydrogenation reaction under same reaction conditions (10 bar H_2, 70 °C) with just the filtrate. As shown in Fig. S34,† after filtration and with one additional hour no further H_2-uptake was detected for the benzene hydrogenation. The CS_2 poisoning experiments and the filtration test provide compelling evidence that Rh@CTF-1 nanomaterial is a truly heterogeneous catalyst which does not seem to act as a reservoir of soluble metal atom or cluster catalysts.

Hydrogen evolution reaction

There is an increasing interest of advanced materials for sustainable hydrogen production from water splitting since hydrogen qualifies as future energy carrier.[88,89] The most effective catalysts for the hydrogen evolution reaction (HER) are Pt group metals.[90] Therefore, we compared Rh@CTF-1 with commercial Pt/C as electrocatalysts for the HER.

Fig. 6a shows the HER polarization curves of Rh@CTF-1 and Pt@CTF-1 synthesized in [BMIm][NTf_2] and commercial Pt/C. To gain insights into the mechanism of the catalytic activity of Rh@CTF-1, Pt@CTF-1 and commercial Pt/C for HER, reaction kinetics were evaluated from the Tafel plots. The Tafel slope of Rh@CTF-1 was calculated to be 37 mV dec^{-1}, which is much lower than that of Pt@CTF-1 (88 mV dec^{-1}; Fig. 6b) and commercial Pt/C (58 mV dec^{-1}; Fig. 6b). The low Tafel slope of Rh@CTF-1 reveals that the rate-limiting step in HER is the Tafel recombination process, *i.e.*, the Volmer–Tafel mechanism. Moreover, at a current density of 10 mA cm^{-2}, the operating potential is measured to be −57 mV for Rh@CTF-1, while Pt@CTF-1 and commercial Pt/C show more negative operating potentials of −111 mV and −77 mV, respectively (Fig. 6c). In addition, Rh@CTF-1 displays an onset potential of −31 mV, which is much more positive than that of Pt@CTF-1 (−44 mV; Fig. 6d) and commercial Pt/C (−38 mV; Fig. 6d). These results demonstrate that Rh@CTF-1 displays a superior HER activity compared to Pt@CTF-1 and commercial Pt/C.

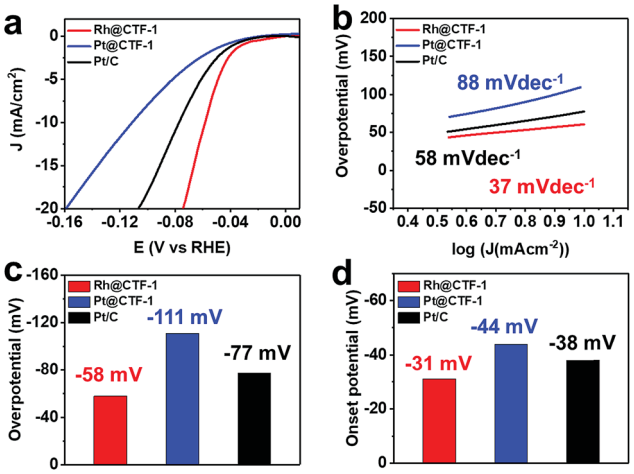

Fig. 6 (a) Polarization curves of Rh@CTF-1, Pt@CTF-1 and commercial Pt/C for HER in 0.5 M H_2SO_4 with a potential scan rate of 20 mV s^{-1}. (b) Corresponding Tafel plots for the data presented in (a). (c) Overpotentials (at current density of 10.0 mA cm^{-2}) of Rh@CTF-1, Pt@CTF-1 and commercial Pt/C. (d) Onset potentials and polarization curves (at current density of 1.0 mA cm^{-2}) of Rh@CTF-1, Pt@CTF-1 and commercial Pt/C. HER experiments with Rh@CTF-1 and Pt@CTF-1 as electrocatalysts was repeated twice to ensure the reproducibility. For repeated HER tests of Rh@CTF-1 and Pt@CTF-1 see Fig. S35 in ESI.†

Conclusions

We describe an easy and rapid method for the synthesis of ruthenium, rhodium, iridium and platinum metal nanoparticles (M-NPs) supported on covalent triazine-based framework, CTF-1 in the ionic liquid (IL) 1-butyl-3-methylimidazolium bis(trifluoromethylsulfonyl)imide ([BMIm][NTf_2]) or in propylene carbonate (PC). In both of the reaction media [BMIm][NTf_2] and PC, very small M-NPs were achieved which are supported on CTF-1 with, *e.g.*, size distributions of 3.0 (±0.5) nm for Ru@CTF-1 synthesized in [BMIm][NTf_2] and 2 (±1) nm for Rh@CTF-1 synthesized in PC.

We see the use of weakly coordinating IL or PC as reaction medium and the non-use of stabilizing capping ligands for the M-NPs as a key to the successful deposition of M-NPs on the CTF. The available, "naked" M-NP surface can thereby interact with coordination sites on the CTF layer. In addition, the IL and PC can exfoliate the CTF layers.

The Rh@CTF-1 composite nanomaterial proved to be a highly active and recyclable heterogeneous catalyst for hydrogenation of benzene to cyclohexane. Benzene hydrogenation reactions with over 99% conversion were achieved under mild (10 bar H_2, 70 °C) and solvent-free conditions with turnover frequencies (TOF) up to ~31 000 h^{-1}. It could be observed that the catalytic efficiency in the first runs are the highest with a more-or-less steady decrease. However, the last runs of the catalytic hydrogenation still resulted to considerable TOF values. The Rh@CTF-1/PC catalyst show higher catalytic activity (~31 000 h^{-1}) in comparison with the catalyst synthesized in [BMIm][NTf_2] (~14 500 h^{-1}). After ten consecutive hydrogenation runs with Rh@CTF-1 as catalyst, there is a leaching effect observed, a growth of the supported Rh-NPs and a reduction of crystallinity of the particles which explain the decrease of the catalytic efficiency evaluated by TOF. In particular, we are aiming to support metal nanoparticles (M-NPs) on different CTFs with stronger anchor groups to avoid leaching effects after catalysis.

Additionally, Rh@CTF-1 is an active electrocatalyst for the industrial relevant hydrogen evolution reaction (HER) with an operating potential of −58 mV and an onset potential of −31 mV for Rh@CTF-1. Compared to Pt@CTF-1 and commercial Pt/C, the results demonstrate that Rh@CTF-1 displays a superior HER activity.

Conflicts of interest

There are no conflicts to declare.

Acknowledgements

Authors are thankful to the Deutsche Forschungsgemeinschaft (DFG) for financial support in the priority project SPP 1708 through grant Ja466/31-1/2 and acknowledge a joint DFG-NSFC (National Natural Science Foundation of China) project (DFG JA466/39-1, NSFC grant 5181101338). We thank the Ernst Ruska-Centre (Forschungszentrum Jülich GmbH, Jülich, Germany) for access to the TEM and technical support under project number ER-C A-060. The authors also gratefully acknowledge technical assistance by the Max-Planck-Institut für Eisenforschung GmbH, Düsseldorf for TEM measurements. We thank Wuhan University of Technology for HER and Mrs Annette Ricken for AAS measurements.

Notes and references

1 H. Bi, X. Tan, R. Dou, Y. Pei, M. Qiao, B. Sun and B. Zong, *Green Chem.*, 2016, **18**, 2216–2221.
2 Y. Wan, C. Chen, W. Xiao, L. Jian and N. Zhang, *Microporous Mesoporous Mater.*, 2013, **171**, 9–13.
3 K. B. Sidhpuria, H. A. Patel, P. A. Parikh, P. Bahadur, H. C. Bajaj and R. V. Jasra, *Appl. Clay Sci.*, 2009, **42**, 386–390.
4 E. T. Silveira, A. P. Umpierre, L. M. Rossi, G. Machado, J. Morais, G. V. Soares, I. J. R. Baumvol, S. R. Teixeira, P. F. P. Fichtner and J. Dupont, *Chem.–Eur. J.*, 2004, **10**, 3734–3740.
5 A. Stanislaus and B. H. Cooper, *Catal. Rev.: Sci. Eng.*, 1994, **36**, 75–123.
6 K. Weissermel and H.-J. Arpe, *Industrial Organic Chemistry*, Wiley-VCH, Weinheim, Germany, 2003.
7 J.-F. Le Page, *Applied Heterogeneous Catalysis: Design, Manufacture, Use of Solid Catalysts*, Technip, Paris, France, 1987.
8 J. Zhang and M. H. Liu, *Chem. Ind. Eng. Prog.*, 2009, **28**, 634–638.
9 R. Marcos Esteban, K. Schütte, D. Marquardt, J. Barthel, F. Beckert, R. Mülhaupt and C. Janiak, *Nano-Struct. Nano-Objects*, 2015, **2**, 28–34.
10 D. Marquardt, C. Vollmer, R. Thomann, P. Steurer, R. Mülhaupt, E. Redel and C. Janiak, *Carbon*, 2011, **49**, 1326–1332.
11 Y. Xiao, Y. Wang, W. Zhou and X. H. Peng, *Chem. J. Chin. Univ.*, 2016, **37**, 786–792.
12 L. O. Nindakova, N. M. Badyrova, V. V. Smirnov and S. S. Kolesnikov, *J. Mol. Catal. A: Chem.*, 2016, **420**, 149–158.
13 X. Yang, L. P. Wu, L. L. Ma, X. J. Li, T. J. Wang and S. J. Liao, *Catal. Commun.*, 2015, **59**, 184–188.
14 E. A. Karakhanov, A. L. Maksimov, E. M. Zakharian, Y. S. Kardasheva, S. V. Savilov, N. I. Truhmanova, A. O. Ivanov and V. A. Vinokurov, *J. Mol. Catal. A: Chem.*, 2015, **397**, 1–18.
15 R. Marcos Esteban, K. Schütte, P. Brandt, D. Marquardt, H. Meyer, F. Beckert, R. Mülhaupt, H. Kölling and C. Janiak, *Nano-Struct. Nano-Objects*, 2015, **2**, 11–18.
16 P. Cao, Y. Q. Ni, R. Zou, L. Q. Zhang and D. M. Yue, *RSC Adv.*, 2015, **5**, 3417–3424.
17 D. Astruc, F. Lu and J. R. Aranzaes, *Angew. Chem., Int. Ed.*, 2005, **44**, 7852–7872.
18 J. A. Widegren and R. G. Finke, *J. Mol. Catal. A: Chem.*, 2003, **191**, 187–207.
19 R. Zou, C. Li, L. Q. Zhang and D. M. Yue, *Catal. Commun.*, 2016, **81**, 4–9.
20 R. Zou, S. P. Wen, L. Q. Zhang, L. Liu and D. M. Yue, *RSC Adv.*, 2015, **5**, 99884–99891.
21 A. Roucoux, J. Schulz and H. Patin, *Chem. Rev.*, 2002, **102**, 3757–3778.
22 F. Bergaya, B. K. G. Theng and G. Lagaly, *Handbook of Clay Science*, Elsevier Publication, The Netherlands, 1st edn, 2006.
23 F. Robert, G. Oehme, I. Grassert and D. Sinou, *J. Mol. Catal. A: Chem.*, 2000, **156**, 127–132.
24 R. Quyoum, V. Berdini, M. L. Turner, H. C. Long and P. M. Maitlis, *J. Catal.*, 1998, **173**, 355–365.
25 O. A. Ferretti, C. Lucas, J. P. Candy, J. M. Basset, B. Didillon and F. Le Peltier, *J. Mol. Catal. A: Chem.*, 1995, **103**, 125–132.
26 P. Kuhn, M. Antonietti and A. Thomas, *Angew. Chem., Int. Ed.*, 2008, **47**, 3450–3453.
27 P. Kuhn, A. Thomas and M. Antonietti, *Macromolecules*, 2009, **42**, 319–326.
28 X. M. Liu, H. Li, Y. W. Zhang, B. Xu, A. Sigen, H. Xia and Y. Mu, *Polym. Chem.*, 2013, **4**, 2445–2448.
29 A. Thomas, A. Fischer, F. Goettmann, M. Antonietti, J. O. Müller, R. Schlögl and J. M. Carlsson, *J. Mater. Chem.*, 2008, **18**, 4893–4908.
30 A. Bhunia, D. Esquivel, S. Dey, R. Fernández-Terán, Y. Goto, S. Inagaki, P. van der Voorta and C. Janiak, *J. Mater. Chem. A*, 2016, **4**, 13450–13457.
31 A. Bhunia, I. Boldog and C. Janiak, *J. Mater. Chem. A*, 2013, **1**, 14990–14999.
32 P. Katekomol, J. Roeser, M. Bojdys, J. Weber and A. Thomas, *Chem. Mater.*, 2013, **25**, 1542–1548.
33 Z. Wang, C. Liu, Y. Huang, Y. Hu and B. Zhang, *Chem. Commun.*, 2016, **52**, 2960–2963.
34 A. V. Bavykina, E. Rozhko, M. G. Goesten, T. Wezendonk, B. Seoane, F. Kapteijn, M. Makkee and J. Gascon, *ChemCatChem*, 2016, **8**, 2217–2221.
35 S. Hug, M. B. Mesch, H. Oh, N. Popp, M. Hirscher, J. Senker and B. V. Lotsch, *J. Mater. Chem. A*, 2014, **2**, 5928–5936.
36 R. Kamai, K. Kamiya, K. Hashimoto and S. Nakanishi, *Angew. Chem., Int. Ed.*, 2016, **55**, 13184–13188.
37 E. Troschke, S. Grätz, L. Borchardt, D. Haubold, I. Senkovska, A. Eychmüller and S. Kaskel, *Microporous Mesoporous Mater.*, 2017, **239**, 190–194.
38 M. Soorholtz, R. J. White, T. Zimmermann, M.-M. Titirici, M. Antonietti, R. Palkovits and F. Schüth, *Chem. Commun.*, 2013, **49**, 240–242.
39 J. Artz and R. Palkovits, *ChemSusChem*, 2015, **8**, 3832–3838.

40 R. Palkovits, M. Antonietti, P. Kuhn, A. Thomas and F. Schüth, *Angew. Chem., Int. Ed.*, 2009, **48**, 6909–6912.
41 T. He, L. Liu, G. Wua and P. Chen, *J. Mater. Chem. A*, 2015, **3**, 16235–16241.
42 J. Artz, S. Mallmann and R. Palkovits, *ChemSusChem*, 2015, **8**, 672–679.
43 C. E. Chan-Thaw, A. Villa, P. Katekomol, D. Su, A. Thomas and L. Prati, *Nano Lett.*, 2010, **10**, 537–541.
44 M. Pilaski, J. Artz, H.-U. Islam, A. M. Beale and R. Palkovits, *Microporous Mesoporous Mater.*, 2016, **227**, 219–227.
45 M. Soorholtz, L. C. Jones, D. Samuelis, C. Weidenthaler, R. J. White, M.-M. Titirici, D. A. Cullen, T. Zimmermann, M. Antonietti, J. Maier, R. Palkovits, B. F. Chmelka and F. Schüth, *ACS Catal.*, 2016, **6**, 2332–2340.
46 K. Kamiya, R. Kamai, K. Hashimoto and S. Nakanishi, *Nat. Commun.*, 2014, **5**, 5040.
47 S. Chen, Y. Zhu, D. Xu, W. Peng, Y. Li, G. Zhang, F. Zhang and X. Fan, *ChemElectroChem*, 2018, **5**, 717–721.
48 K. Leus, K. Folens, N. R. Nicomel, J. P. H. Perez, M. Filippousi, M. Meledina, M. M. Dîrtu, S. Turner, G. Van Tendeloo, Y. Garcia, G. Laing and P. Van Der Voort, *J. Hazard. Mater.*, 2018, **353**, 312–319.
49 J. D. Makinson, J. S. Lee, S. H. Magner, R. J. de Angelis, W. N. Weins and A. S. Hieronymus, *Adv. X-Ray Anal.*, 2000, **42**, 407–411.
50 M. Kurian and C. Kunjachan, *Nano-Struct. Nano-Objects*, 2015, **1**, 15–23.
51 F. Zhang, S.-W. Chan, J. E. Spanier, E. Apak, Q. Jin, R. D. Robinson and I. P. Herman, *Appl. Phys. Lett.*, 2002, **80**, 127–129.
52 K. M. Reddy, S. V. Manorama and A. R. Reddy, *Mater. Chem. Phys.*, 2003, **78**, 239–245.
53 M. Manhas, V. Kumar, V. Sharma, O. M. Ntwaeaborwa and H. C. Swart, *Nano-Struct. Nano-Objects*, 2015, **3**, 9–16.
54 Ernst Ruska-Centre for Microscopy and Spectroscopy with Electrons, *Journal of Large-Scale Research Facilities*, 2017, **2**, A77.
55 A. Thust, J. Barthel and K. Tillmann, *Journal of Large-Scale Research Facilities*, 2016, **2**, A41.
56 J. Barthel and A. Thust, *Phys. Rev. Lett.*, 2008, **101**, 200801.
57 C. L. Jia, L. Houben, A. Thust and J. Barthel, *Ultramicroscopy*, 2010, **110**, 500–505.
58 F. Zemlin, K. Weiss, P. Schiske, W. Kunath and K. H. Herrmann, *Ultramicroscopy*, 1978, **3**, 49–60.
59 A. Bhunia, S. Dey, M. Bous, C. Zhang, W. von Rybinski and C. Janiak, *Chem. Commun.*, 2015, **51**, 484–486.
60 J. Zhou, D. Zhang, X. Zhang, H. Song and X. Chen, *ACS Appl. Mater. Interfaces*, 2014, **6**, 21223–21229.
61 S. Wolf, W. Klopper and C. Feldmann, *Chem. Commun.*, 2018, **54**, 1217–1220.
62 S. Santner, S. Yogendra, J. J. Weigand and S. Dehnen, *Chem.–Eur. J.*, 2017, **23**, 1999–2004.
63 M. F. Groh, U. Müller, E. Ahmed, A. Rothenberger and M. Ruck, *Z. Naturforsch., B: J. Chem. Sci.*, 2013, **68**, 1108–1122.
64 R. Elfgen, O. Hollóczki and B. Kirchner, *Acc. Chem. Res.*, 2017, **50**, 2949–2957.
65 M. Siebels, L. Mai, L. Schmolke, K. Schütte, J. Barthel, J. Yue, J. Thomas, B. M. Smarsly, A. Devi, R. A. Fischer and C. Janiak, *Beilstein J. Nanotechnol.*, 2018, **9**, 1881–1894.
66 K. Klauke, D. H. Zaitsau, M. Bülow, L. He, M. Klopotowski, T.-O. Knedel, J. Barthel, C. Held, S. P. Verevkin and C. Janiak, *Dalton Trans.*, 2018, **47**, 5083–5097.
67 C. Janiak, *Z. Naturforsch., B: J. Chem. Sci.*, 2013, **68**, 1059–1089.
68 B. Schäffner, S. P. Verevkin and A. Börner, *Chem. Unserer Zeit*, 2009, **43**, 12–21.
69 B. Schäffner, F. Schäffner, S. P. Verevkin and A. Börner, *Chem. Rev.*, 2010, **110**, 4554–4581.
70 K. Schütte, J. Barthel, M. Endres, M. Siebels, B. Smarsly, J. Yue and C. Janiak, *ChemistryOpen*, 2017, **6**, 137–148.
71 A. P. Umpierre, E. de Jesffls and J. Dupont, *ChemCatChem*, 2011, **3**, 1413–1418.
72 J. L. Anthony, E. J. Maginn and J. F. Brennecke, *J. Phys. Chem. B*, 2002, **106**, 7315–7320.
73 S. H. Barghi, T. T. Tsotsis and M. Sahimi, *Int. J. Hydrogen Energy*, 2005, **40**, 8713–8720.
74 G. A. Somorjai and J. Y. Park, *Top. Catal.*, 2008, **49**, 126–135.
75 X. Zhou, W. Xu, G. Liu, D. Panda and P. Chen, *J. Am. Chem. Soc.*, 2010, **132**, 138–146.
76 X. Kang, J. Zhang, W. Shang, T. Wu, P. Zhang, B. Han, Z. Wu, G. Mo and X. Xing, *J. Am. Chem. Soc.*, 2014, **136**, 3768–3771.
77 H. Liu, R. Fang, Z. Li and Y. Li, *Chem. Eng. Sci.*, 2015, **122**, 350–359.
78 W. Alsalahi, W. Tylus and A. M. Trzeciak, *ChemCatChem*, 2018, **10**, 2051–2058.
79 A. Sánchez, M. Fang, A. Ahmed and R. A. Sánchez-Delgado, *Appl. Catal., A*, 2014, **477**, 117–124.
80 M. N. Shaikh, M. A. Aziz, A. N. Kalanthoden, A. Helal, A. S. Hakeem and M. Bououdina, *Catal. Sci. Technol.*, 2018, **8**, 4709–4717.
81 S. Akbayrak, *J. Colloid Interface Sci.*, 2018, **530**, 459–464.
82 C. Vollmer, E. Redel, K. Abu-Shandi, R. Thomann, H. Manyar, C. Hardacre and C. Janiak, *Chem.–Eur. J.*, 2010, **16**, 3849–3858.
83 L. Durán Pachón and G. Rothenberg, *Appl. Organomet. Chem.*, 2008, **22**, 288–299.
84 C. M. Hagen, J. A. Widegren, P. M. Maitlis and R. G. Finke, *J. Am. Chem. Soc.*, 2005, **127**, 4423–4432.
85 B. J. Hornstein, J. D. Aikon III and R. G. Finke, *Inorg. Chem.*, 2002, **41**, 1625–1638.
86 Y. Lin and R. G. Finke, *Inorg. Chem.*, 1994, **33**, 4891–4910.
87 J. A. Widegren, M. A. Bennett and R. G. Finke, *J. Am. Chem. Soc.*, 2002, **124**, 10301–10310.
88 M. G. Walter, E. L. Warren, J. R. McKone, S. W. Boettcher, Q. Mi, E. A. Santori and N. S. Lewis, *Chem. Rev.*, 2010, **110**, 6446–6473.
89 M. S. Dresselhaus and I. L. Thomas, *Nature*, 2001, **414**, 332–337.
90 S. Trasatti, *Adv. Electrochem. Sci. Eng.*, 1992, **2**, 1–86.